Differences in the Response of Additively Manufactured Titanium Alloy to Heat Treatment – Comparison between SLM and EBM

Michaela Roudnicka, Michal Misurak, Dalibor Vojtech
Department of Metals and Corrosion Engineering, Faculty of Chemical Technology, University of Chemistry and technology Prague, Technicka 5, 166 28 Prague 6 – Dejvice, Czech Republic. E-mail: michaela.roudnicka@vscht.cz, misurakm@vscht.cz, vojtechd@vscht.cz

Additive manufacturing (AM) of metals is expanding and already starts to reach industrial scale. Among many different technologies of AM, powder-bed technologies are the most widespread as they provide the highest resolution and so the widest options in the production of complex parts. Selective laser melting (SLM) and electron beam melting (EBM) both belong to this technological group. In this paper, we describe the differences between these two technologies on the example of titanium alloy production. Due to different material states in the as-built condition, the material shows a different response to heat treatment. We depict the differences by microstructure observations and hardness measurement after annealing the titanium alloy at temperatures of 100-1000 °C and subsequent water quenching. While the titanium alloy is stable when manufactured by EBM, it shows microstructural changes associated with changes in mechanical properties when manufactured by SLM.

Keywords: Titanium alloy, Additive manufacturing, SLM, EBM, Heat treatment

1 Introduction

Although 3D printing of metals, as additive manufacturing (AM) is familiarly called, is still often seen by the general public as science fiction, it already starts to reach industrial scale. Among many different technologies of AM, powder-bed technologies are the most widespread as they provide the highest resolution and so the widest options in the production of complex parts [1].

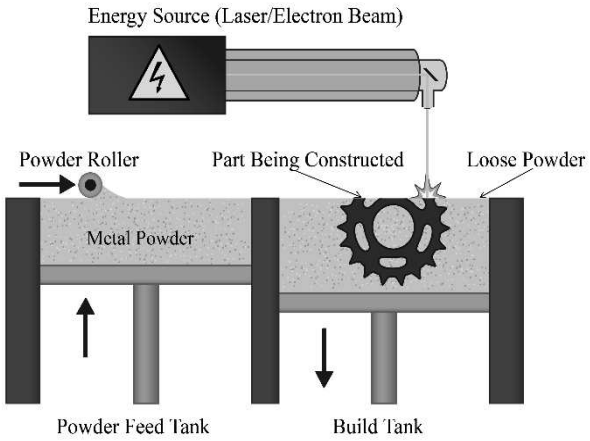

Fig. 1 *Schema of powder bed AM technologies[3].*

Powder-bed technologies work with fine powder materials with particles of tens micrometres in size. That is one of the prerequisites for their high resolution. Contrary to direct deposition technologies, where the powder is deposited already in the shape of the desired product, in powder-bed technologies, the powder is successively deposited in thin layers onto a building plate in a working chamber and forms a 'powder bed', within which a product is built afterwards. The fusion of powder particles occurs by selective irradiation by an energy source, which can be a laser or electron beam. In each step, a layer of tens micrometres in thickness is processed. After that, the building plate is lowered, a new powder is deposited and the next layer of the product is built. For such layer-wise production, the product must be computer-sliced and two-dimensional coordinates obtained for all layers. The third dimension is then given by the shift of the building plate, which is determined by the thickness of a deposited layer [2]. A simplified schema showing the principle of powder-bed technologies is given in Fig. 1.

Selective laser melting (SLM) and electron beam melting (EBM) both belong to this technological group. The main difference between these two technologies lies in the energy source, which is a laser beam for SLM and an electron beam for EBM. Due to the use of electrons, EBM must work under vacuum, while an inert atmosphere is fed to the SLM chamber. An electron beam is generally of a much higher power, therefore, it usually works with larger powder particles and higher layer thickness. Also, significantly faster scanning rates can be used. Nevertheless, it does not necessarily mean that the EBM process is faster. In EBM, a pre-scan is applied to each layer to heat the powder up to reduce temperature gradients and great thermal stresses which would negatively affect part build-up. That prolongs the process. In SLM systems, only the building plate can be preheated, not the whole 'powder bed'. SLM thus yields products with significant internal stresses, which are usually desirable to be removed by additional heat treatment of the products [4]. After EBM, no heat treatment is generally necessary [5]. The comparison of the main features of SLM and EBM is given in Tab. 1.

Titanium and its alloys are an expensive material, not only due to the high price of the raw material but also because of difficulty in processing under a protective atmosphere and difficult machining. Conventional manufacturing methods result in high manufacturing costs as the part production requires many operations, many tools and is accompanied by a significant material loss. By minimizing both material loss and production steps, AM thus rep-

resents a great opportunity in titanium production. Moreover, thanks to their great strength-to-weight ratio, corrosion resistance and biocompatibility, titanium and its alloys are one of the main materials used for demanding and high-performance applications, such as various industrial components, engine parts, medical implants etc. Components for such applications often require specific complex shapes. Here, AM also extends the present possibilities and brings novel designs [1, 6].

Tab. 1 *Comparison between SLM and EBM [6-8]*

	SLM	**EBM**
Energy source	laser	electron beam
Beam size	0.1-0.5 mm	0.2-1.0 mm
Scanning	galvanometers	deflection coils
Energy absorption	absorptivity-limited	conductivity-limited
Resolution	0.04-0.2 mm	0.1 mm
Accuracy	±0.05-0.2 mm	±0.2 mm
Working environment	inert atmosphere (Ar, N_2)	vacuum
Preheating	resistive heating of the building plate	powder bed pre-heating by electron beam
Layer thickness	30-100 μm	50-200 μm
Scanning speed	< 10 m/s	< 8000 m/s
Build rate	< 50 cm^3/h	55-80 cm^3/h
Surface finish	Ra 9-12 μm	Ra 25-35 μm
Residual stresses	high	minimal
Heat treatment	stress relief required	not required

A huge amount of scientific literature illustrates the interest in the AM of titanium. Many research works have focused on the optimization of SLM/EBM process parameters to reach the highest possible density (e.g. [9, 10]), others have developed and tested various complex structures prepared by AM (e.g. [11, 12]), some were focused on treating the surface of additively manufactured titanium to reduce relatively high surface roughness and improve related properties (e.g. [13, 14]), etc. There have also been papers directly comparing various properties of titanium alloys manufactured by SLM, on one hand, and by EBM on the other (e.g. [15, 16]). Although similar results can be achieved by SLM and EBM after some minor modifications (such as stress relief after SLM, surface treatment etc.), there are some process-inherent differences encoded in the as-printed material. In this paper, we digestedly describe the differences in the structure of the titanium alloy Ti-6Al-4V processed by SLM and EBM, and different responses to heat treatment associated with them.

2 Experimental Setup

2.1 Samples preparation

The material studied in this paper is the Ti-6Al-4V alloy (grade 23 ELI) of the composition listed in Tab. 2. For the purpose of additive manufacturing, it is used in the form of a gas-atomized powder with particles of spherical shape and suitable particle size distribution. The powders were purchased from industrial suppliers recommended for each AM technology. For selective laser melting (SLM), it was rematitan® CL (Dentaurum, Germany) powder with the particle size of 15-45 μm. Since electron beam melting (EBM) operates with higher energies, larger particles are suitable. Powder of 45-105 μm particle size was purchased from AP&C.

Tab. 2 *The composition of Ti-6Al-4V alloy, grade 23 ELI (ASTM F2924, wt.%)*

Ti	**Al**	**V**	**Fe**	**O**	**C**	**N**	**H**
bal.	5.50 – 6.75	3.50 – 4.50	max. 0.30	max. 0.20	max. 0.10	max. 0.05	max. 0.015

Selective laser melting was carried on an M2 Cusing machine, ConceptLaser. This machine is equipped with one Yb:YAG fibre laser of 200 W in power. Samples in the form of round bars, 0.5 mm in diameter and 90 mm in length, were fabricated with a laser power of 200 W, scanning speed of 0.8 m/s and hatching distance of 112 μm. Samples were fabricated by the processing of 30 μm thin layers of the powder gradually deposited by a rake onto the building plate. Each layer was scanned with the use of an 'island' scanning strategy in which 'islands' of 5x5 mm^2 in size are scanned in a random order to minimize the formation of steep thermal gradients and so internal stresses. Samples were built in the vertical orientation. Argon was fed to the building chamber to prevent oxidation. Final samples were cut into cylinders of 10 mm in height for the subsequent tests of heat treatment influence.

Electron beam melting was accomplished on an Arcam Q10 EBM machine, which operates under vacuum with an electron beam of 3000 W in max. power. A block of 40x20x20 mm^3 was fabricated and subsequently cut into cubic samples with an edge of 10 mm. The block was fabricated in 50 μm thin layers which were deposited by a rake onto the building platform continuously heated to 740 °C by a rapid scan (10 m/s) of the electron beam with a beam current of 30 mA. In each layer, the powder was selectively melted by the electron beam, with a beam current of 15 mA, scanned in lines across the building plate by a speed of 4.5 m/s. The hatching distance between lines was 0.2 mm.

2.2 Heat treatment

Prepared samples were annealed in a muffle furnace Martinek MP05 at temperatures of 100 to 1000 °C. Annealing at each temperature was carried out for 2 h. Afterwards, the samples were quenched into water. The influence of annealing on hardness and microstructure evolution was observed.

Hardness was measured on samples ground on SiC paper P2500 using a Vickers hardness tester Future-Tech FM-700 and 1 kg load applied for 10 s. Hardness was measured, both prior and after the annealing, for each sample to observe hardness change due to annealing only and eliminate the effect of a possible microstructural anisotropy. Hardness values were statistically evaluated from 10 measurements.

Microstructure in the as-built states and after annealing was observed using an inverted optical microscope Olympus PME3 and a scanning electron microscope TESCAN VEGA-3 LMU. The samples were ground, polished on diamond pastes and silica suspension supplemented with hydrogen peroxide, and etched in Kroll's reagent.

3 Results and Discussion

3.1 Influence of additive manufacturing technology

Figure 2 represents the differences between the microstructures of Ti-6Al-4V alloy prepared by SLM (Fig. 2 a-c) and EBM (Fig. 2 d-f). On longitudinal sections (Fig. 2 a,d), columnar grains elongated in the building direction can be seen in both samples. The epitaxial growth of grains across many successively deposited layers is the result of laser remelting of several previously processed layers. New grains thus nucleate in the same crystallographic orientation as grains in previous layers [17]. During cooling, the high-temperature β-phase transforms. Cooling rates during SLM/EBM can reach up to 10^5-10^6 °C/s [17]. At such rates, diffusionless martensitic transformation occurs. The prior β grains are thus filled with martensitic needles. Until this point, the microstructure evolution is the same in SLM and EBM but, as it is clear on the comparison of Figs. 1c and 1f, the final microstructure is different [18, 19]. Conversely to SLM, the EBM building chamber is preheated each layer, which reduces thermal stresses in the material and eliminates the need for annealing final products. Considering the temperature of preheating (740 °C) is higher than the temperature needed for martensite decomposition (575 °C [20]), martensitic phase transforms into the mixture of α+β phases. Vanadium atoms diffuse from the martensitic needles which become lamellae of α-phase, and β-phase is formed in the interlamellar space. Compared to the single-phase and very fine needle-like microstructure of the SLM Ti-6Al-4V alloy (Fig. 2c), the EBM samples thus show two-phase coarser lamellar microstructure (Fig. 2f).

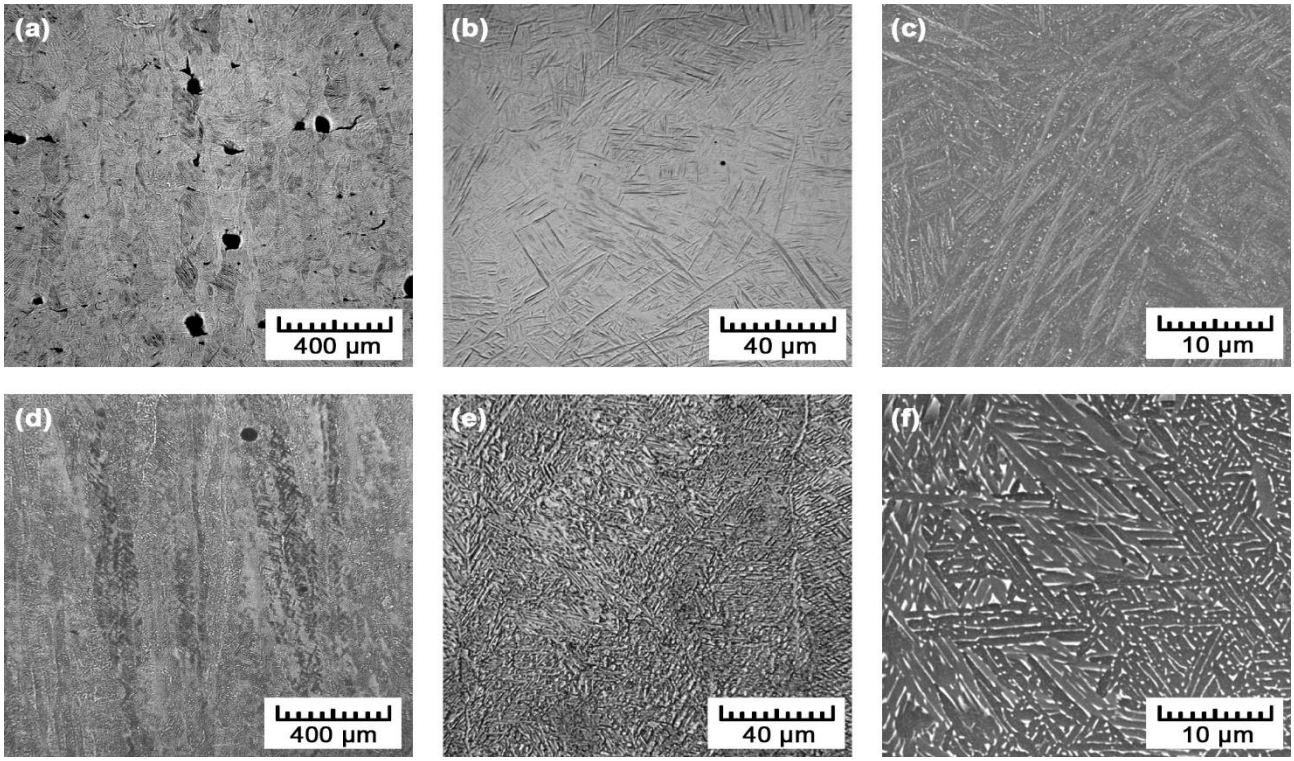

Fig. 2 *Microstructures of Ti-6Al-4V prepared by a-c) SLM, d-f) EBM.*

Hardness measured in the as-built state showed slightly different values than could be expected. Although higher hardness could be expected for SLM samples with finer martensitic structure and high level of internal stresses, we obtained a value of 342 ± 5 HV1 compared to 375 ± 5 HV1 for EBM samples. Such a discrepancy can be caused by porosity. SLM samples showed porosity of 1.7 ± 0.5% while EBM material was almost defect-free (porosity of 0.2 ± 0.1%). The pores observed in the SLM samples (Fig. 3a) suggest insufficient fusion in between successively melted scan tracks. These so-called lack-of-fusion (LOF) defects are of an irregular shape, elongated

in the scanning direction and distributed along the scan tracks. Higher energy should bet thus delivered to the powder material to ensure its proper consolidation. EBM is generally associated with much higher energy. Therefore, no LOF was observed (Fig. 3b). The 0.2% porosity was represented by smaller spherical pores formed by gas entrapment. At a high solidification rate, gas might not be able to escape from the melt and forms gas bubbles. Also, it is possible that the material itself evaporates at high energy and spherical voids are then formed. This phenomenon is known as the key-hole effect [21].

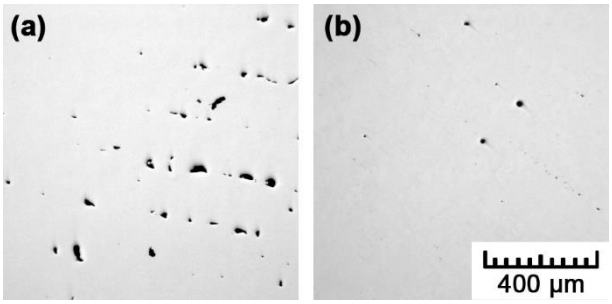

Fig. 3 *Porosity of Ti-6Al-4V samples: a) SLM, b) EBM*

3.2 Influence of heat treatment

Figure 4 shows the hardness evolution with annealing the samples at different temperatures. There is a remarkable difference between SLM and EBM. While, for SLM, we observed a peak at 600 °C, no significant hardness changes were registered for EBM. Different response of the material to annealing is related to the different microstructure in the as-built state. While α+β lamellar microstructure is relatively stable up to the transformation temperature (995±5 °C [22]), martensite decomposes during annealing.

When we compare the SLM microstructure in the as-built state (Fig. 5a) and after annealing at 600 °C (Fig. 5b), we observe martensitic needle-like microstructure with no significant difference. The changes that occur take place on a nanometer scale and can be visualized only by transmission electron microscopy. Wu et al. [22] showed in their paper that the hardness increase is associated with the gradual decomposition and refinement of martensitic needles. Above 600 °C, martensite starts to decompose into the mixture of α+β phases state (Fig. 5c). The higher the temperature, the more martensite is transformed and the hardness decreases. Microstructure coarsens, stresses are relieved. At temperatures above 900 °C (martensite start), β phase undergoes shear transformation into martensite again. A combined α-lamellar microstructure with small amount of martensitic needles can be formed. Above the transformation temperature, the whole material is in the state of the β phase so that quenching results in a fully martensitic microstructure. Above 900 °C, hardness can be expected to increase. Nevertheless, at such high temperatures, titanium is very prone to oxygen which affects its properties and transformation temperatures. Due to annealing under atmospheric conditions, increased amount of oxygen dissolved in the solid solution probably shifted the martensite start temperature Ms towards higher values [23]. Therefore, the lamellar two-phase microstructure can be still observed (Fig. 5d). Compared to the micrograph for a lower temperature of 800 °C (Fig. 5c), we can see that the lamellae have coarsened.

In the EBM samples, an equilibrium α+β lamellar microstructure is already present in the as-built state (Fig. 5e). Martensite transformation, which occurs above 600 °C in the SLM samples, already took place during the EBM process at the preheating temperature of 740 °C. No significant hardness change was measured up to 900 °C (Fig. 4b). Hardness only slightly gradually decreased due to a gradual coarsening of α-lamellae (Fig. 5e-g). Similarly to the SLM samples, at temperatures around 1000 °C, there was already a significant oxygen affection. In an oxygen-free atmosphere, the martensitic transformation would already take place during quenching but here we observed a lamellar two-phase structure (Fig. 5h). Due to the strengthening effect of oxygen dissolved in the solid solution, hardness rose at 1000 °C (Fig. 4b).

On the comparison of microstructures obtained after annealing the SLM and EBM samples (Fig. 5), it can be noticed that the microstructure of the SLM and EBM samples was comparable after annealing at 800 °C. A comparable hardness was achieved too (Fig. 5). As a temperature of 820 °C is usually recommended to relieve stresses and stabilize the microstructure after SLM, one can see that a final material state is similar regardless of the applied AM technology.

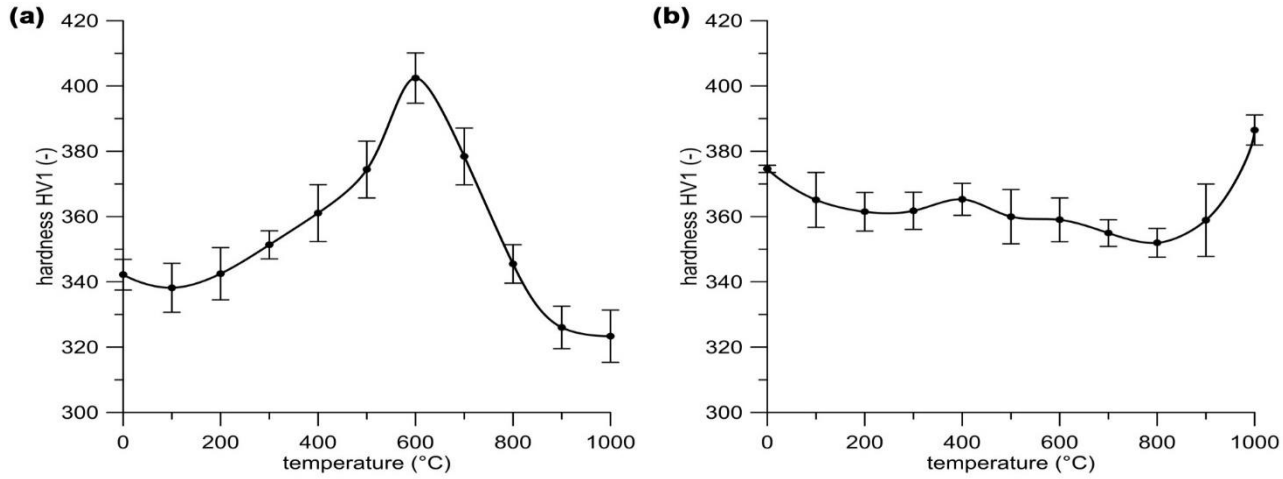

Fig. 4 *Hardness evolution during annealing Ti-6Al-4V samples produced by: a) SLM, b) EBM*

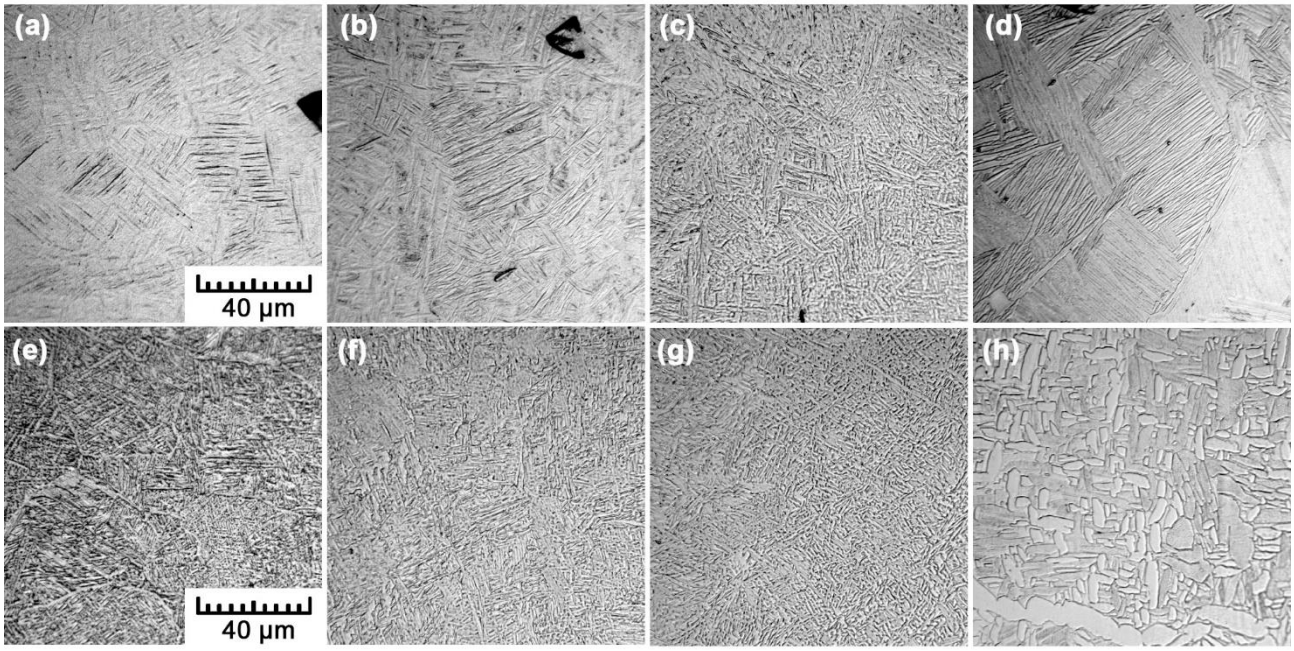

Fig. 5 *Microstructure changes at different annealing temperatures: a) SLM as-built, b) SLM-600°C, c) SLM-800 °C, d) SLM-1000 °C, e) EBM as-built, f) EBM-600 °C, g) EBM-800 °C, h) EBM-1000 °C. Same scale for all micrographs.*

4 Conclusion

Although SLM and EBM technologies are based on the same principle of melting the powder deposited in thin layers into the working chamber, they show some differences resulting in the material of different microstructure and behaviour. Melting small volumes of powder material by a focused laser or electron beam yields extreme cooling rates at which Ti-6Al-4V alloy undergoes a martensitic transformation. In SLM, which works at ambient temperature, martensitic microstructure is preserved in the final as-built samples. However, preheating of the material in the EBM working chamber is responsible for the transformation into a stable α+β lamellar microstructure. The different as-built state is then the cause of different material response to heat treatment. We observed material changes associated with the decomposition of the metastable martensitic phase during annealing the SLM samples. The maximum hardness was reached after annealing the samples at 600 °C followed with water-quenching. Compared to that, the microstructure and hardness were stable for the EBM samples.

Acknowledgement

Authors wish to thank the Czech Ministry of Education, Youth and Sports for the financial support for specific university research (MSMT No. 21-SVV/2019). Thanks also belongs to Prospon spol. s r. o., Czech Republic and Metal Industries Research & Development Centre, Taiwan for providing the testing material.

References

[1] DUDA, T., RAGHAVAN, L. V. (2016). 3D Metal Printing Technology. In: *IFAC-PapersOnLine*, Vol. 49, No. 29, pp. 103-110.

[2] HERZOG, D., SEYDA, V., WYCISK, E., EMMELMANN, C. (2016). Additive manufacturing of metals. In: *Acta Materialia*, Vol. 117, pp. 371-392.

[3] 3DEO (2018). *Intro to Metal 3D Printing Processes - Powder Bed Fusion (DMLS, SLS, SLM, LMF, DMP, EBM)*. [cited 21. 8. 2019]; Available from: https://news.3deo.co/metal-3d-printing-processes-powder-bed-fusion-dmls-sls-slm-lmf-dmp-ebm.

[4] FOUSOVA, M., VOJTECH, D. (2018). Thermal treatment of 3D-printed Titanium alloy. In: *Manufacturing Technology*, Vol. 18, No. 2, pp. 227-232.

[5] RAHMAN, M. S., SCHILLING, P. J., HERRINGTON, P. D., CHAKRAVARTY, U. K. (2019). A Comparative Study Between Selective Laser Melting and Electron Beam Additive Manufacturing Based on Thermal Modeling. In: *ASME 2018 International Mechanical Engineering Congress and Exposition*.

[6] AGAPOVICHEV, A., SOTOV, A., KOKAREVA, V., SMELOV, V. (2018). Possibilities and limitations of titanium alloy additive manufacturing. In: *MATEC Web of Conferences* (*ICMTMTE 2018),* Vol. 224. Article no. 01064.

[7] BÁRTOLO, P. J. S., Kruth, J. P., DA SILVA, J. V. L., LEVY, G., MALSHE, A. P., RAJURKAR, K. P., MITSUISHI, M., CIURANA, J., LEU, M. CH. (2012) Biomedical production of implants by additive electro-chemical and physical processes. In: *CIRP Annals*, Vol. 61, No. 2, pp. 635-655.

[8] ADDITIVELY. [cited 21. 8. 2019]; Available from: https://www.additively.com/en/learn-about.

[9] WANG, Z., XIAO, Z., TSE, Y., HUANG, C., ZHANG, W. (2019). Optimization of processing parameters and establishment of a relationship between microstructure and mechanical properties of SLM titanium alloy. In: *Optics & Laser Technology*, Vol. 112, pp. 159-167.

[10] MORITA, T., TSUDA, C., NAKANO, T. (2017). Influences of scanning speed and short-time heat treatment on fundamental properties of Ti-6Al-4V alloy produced by EBM method. In: *Materials Science and Engineering: A*, Vol. 704, pp. 246-251.

[11] TAKEZAWA, A., YONEKURA, K., KOIZUMI, Y., ZHANG, X., KITAMURA, M. (2018). Isotropic Ti–6Al–4V lattice via topology optimization and electron-beam melting. In: *Additive Manufacturing*, Vol. 22, pp. 634-642.

[12] QI, D., YU, H., LIU, M., HUANG, H., XU, S., XIA, Y., QIAN, G., WU, W. (2019). Mechanical behaviors of SLM additive manufactured octet-truss and truncated-octahedron lattice structures with uniform and taper beams. In: *International Journal of Mechanical Sciences*. In press.

[13] PYKA, G., BURAKOWSKI, A., KERCKHOFS, G., MOESEN, M., BAEL, S. V., SCHROOTEN, J., WEVERS, M. (2012). Surface Modification of Ti6Al4V Open Porous Structures Produced by Additive Manufacturing. In: *Advanced Engineering Materials*, Vol. 14, No. 6, pp. 363-370.

[14] PERSENOT, T., BUFFIERE, J.-Y., MAIRE, E., DENDIEVEL, R., MARTIN, G. (2017). Fatigue properties of EBM as-built and chemically etched thin parts. In: *Procedia Structural Integrity*, Vol. 7, No., pp. 158-165.

[15] FOUSOVÁ, M., VOJTĚCH, D., DOUBRAVA, K., DANIEL, M., LIN, C.-F. (2018). Influence of Inherent Surface and Internal Defects on Mechanical Properties of Additively Manufactured Ti6Al4V Alloy: Comparison between Selective Laser Melting and Electron Beam Melting. In: *Materials*, Vol. 11, No. 4, pp. 537.

[16] ZHAO, X., LI, S., ZHANG, M., LIU, Y., SERCOMBE, T. B., WANG, S., HAO, Y., YANG, R., MURR, L. E. (2016). Comparison of the microstructures and mechanical properties of Ti–6Al–4V fabricated by selective laser melting and electron beam melting. In: *Materials & Design*, Vol. 95, pp. 21-31.

[17] LIU, S., SHIN, Y. C. (2019). Additive manufacturing of Ti6Al4V alloy: A review. In: *Materials & Design*, Vol. 164, pp. 107552.

[18] FOUSOVA, M., VOJTECH, D. (2018). Possibilities of Electron Beam Melting technology: Titanium processing. In: *Manufacturing Technology*, Vol. 18, No. 3, pp. 387-393.

[19] FOUSOVA, M., VOJTECH, D., KUBASEK, J. (2016). Titanium alloy Ti-6Al-4V prepared by Selective Laser Melting (SLM). In: *Manufacturing Technology*, Vol. 16, No. 4, pp. 691-697.

[20] XU, W., BRANDT, M., SUN, S., ELAMBASSERIL, J., LIU, Q., LATHAM, K., XIA, K., QIAN, M. (2015). Additive manufacturing of strong and ductile Ti–6Al–4V by selective laser melting via in situ martensite decomposition. In: *Acta Materialia*, Vol. 85, pp. 74-84.

[21] KAPLAN, A. (2017). Pores and Inclusions. In: *The Theory of Laser Materials Processing: Heat and Mass Transfer in Modern Technology* (J. Dowden and W. Schulz, (Eds.)), p. 256. Springer International Publishing, Switzerland.

[22] WU, S. Q., LU, Y. J., GAN, Y. L., HUANG, T. T., ZHAO, C. Q., LIN, J. J., GUO, S., LIN, J. X. (2016). Microstructural evolution and microhardness of a selective-laser-melted Ti–6Al–4V alloy after post heat treatments. In: *Journal of Alloys and Compounds*, Vol. 672, pp. 643-652.

SHA, W., MALINOV, S. (2009). *Titanium Alloys: Modelling of Microstructure, Properties and Applications*. Woodhead Publishing Limited, Cambridge.

10.21062/ujep/353.2019/a/1213-2489/MT/19/4/668